MURA 43

MURA-KRS-6

THE FFAG SYNCHROTRON - MARK I*

K. R. Symon

Wayne University and Midwestern Universities Research Association

November 12, 1954

Abstract.

A general description of the fixed field alternating gradient synchrotron is presented, followed by a detailed treatment of orbit geometry, linear orbit theory, and magnetic field patterns for the Mark I machine. Tables of design parameters are worked out for a 10 Bev proton synchrotron.

*This work was supported by the National Science Foundation and MURA.

1. General description.

In the fixed field alternating gradient synchrotron, the magnetic field is kept constant in time, and the magnetic field pattern is so designed that stable orbits of all energies from the injection energy to the output energy are accommodated within the evacuated donut. The required momentum compaction is achieved by arranging that the high energy orbits shall pass through regions of high average magnetic field, and the low energy orbits, through regions of low average magnetic field. In most FFAG machines so far considered, this is accomplished by utilizing magnetic fields whose magnitudes increase rapidly with radius, so that the low energy orbits lie on the inside of the donut, and the high energy orbits, on the outside. It is possible, however, to have stable orbits with negative momentum compaction, so that the high energy orbits are on the inside, and this has several advantages. Stability of horizontal and vertical betatron oscillations is maintained by alternating gradient focussing. In most of the machines that have been proposed, acceleration of the particles is by means of r.f. voltages applied to one or more accelerating gaps around the donut. Phase stability, as in the conventional A.G. synchrotron, allows the particles to be carried from injection energy to output energy by modulating the frequency of the accelerating voltage.

In most of the proposed machines, the circumference of the donut is divided into N sectors, each sector consisting of a radial focussing (vertical defocussing) half-sector, and a radial defocussing (vertical focussing) half sector. In both half-sectors, the magnitude of the magnetic field increases rapidly with radius, and the reverse gradient in the vertical focussing half-sector is obtained

by reversing the direction of the magnetic field. This implies, of course, that the orbit will bend alternately outward and inward in alternate half-sectors, with a consequent increase in the overall circumference of the machine. The ratio between the length of the highest energy orbit, and the circumference of a circle whose radius is the minimum radius of curvature of the highest energy (equilibrium) orbit, is called the circumference factor.

In the Mark I machine, the fields in focussing and defocussing half-sectors increase according to the same function of radius (strictly speaking, of energy), so that the ratio of fields in alternate half-sectors along a given orbit is constant, independent of energy. In order to minimize the circumference factor, one would like to make the vertical focussing sectors have as short a length and as weak a field as possible, but a limit is set here by the requirement of stability of vertical betatron oscillations. It turns out that the maximum ratio of the product of field gradient by sector length between radial and vertical focussing half-sectors is about 3/2. In the Mark Ib machine, the fields are equal and opposite in the two sectors, the sector lengths are in the ratio 3/2, and the resulting circumference factor is 5. In the Mark Ia machine, the half-sector lengths are equal, and the magnetic fields are in the ratio 3/2; the circumference factor is then 6. In Mark I type machines, the half-sector lengths, measured in radians subtended at the center of the machine, are the same for all orbits, and all orbits have similar shapes. In some other types of proposed machines, the half-sector lengths vary with orbit energy, and the different orbits are not geometrically similar. The Mark I machines are the simplest and easiest to analyze mathematically, and this report will be confined to this case, although some of the analysis

will apply to more general types.

It is clear that the FFAG synchrotron, if a practical design can be achieved, will have a number of important advantages over the conventional synchrotrons. The use of D.C. magnets results in a considerable simplification of magnet power supply, allows the use of cheaper grade iron, eliminates remanent field problems, simplifies saturation problems, and allows D.C. trimming for magnet misalignments and imperfections. The necessity for accurate tracking of accelerating voltage frequency with magnetic field rise is eliminated, with a resulting greater freedom and simplicity in the design of the r.f. system, and a possibility of increasing the output current by using high pulse repetition rates. The only restrictions on the frequency modulation cycle are that the frequency must not change too rapidly for the particle energy to follow, and that the r.f. noise be kept small, and even the latter requirement is less severe in the FFAG synchrotron since phase oscillations of any finite amplitude can be accomodated within the donut. Because of the great momentum compaction, the transition energy is much higher than in the conventional A-G synchrotron; in all the designs that we have studied, the transition energy turns out to be above the output energy of the machine, so that the transition energy problem is also eliminated. One can make use of the adiabatic damping of vertical betatron oscillations to design the donut cross section and magnet gap so that the vertical aperture is large at injection and small at high energies, with consecuent saving in iron, and relaxing of injection tolerance. A further simplification of injection problems can be achieved by going to very low injection energies; the only significant penalty paid for low injection energies is an

increase in the range of frequency modulation required, and there are schemes by which this difficulty can be surmounted. Another advantage is that a target may be placed in the machine at the orbit corresponding to the desired energy without the necessity for special schemes to deflect the beam into the target.

The principal disadvantage of the FFAG synchrotron which has so far come to light is the large circumference factor. For the Mark Ib, the circumference factor is 5. However the maximum field on the equilibrium orbit can be made higher in the FFAG synchrotron than in the conventional A.G. synchrotron, both because it is possible to operate the magnet iron well into saturation at the high field points, and because the highest energy orbit lies at the outside edge of the field in the FFAG machine, whereas it lied in the center of the field in the conventional machine. For these reasons, it is probable that the maximum field on the equilibrium orbit in the FFAG synchrotron can be made greater by a factor of perhaps 3/2. The Mark I synchrotron will then be larger in circumference than a conventional machine of the same energy by a factor of 3.3. Other types of FFAG synchrotrons with smaller circumference factors are being studied and will be the subject of future reports.

2. Orbit geometry.

We will use subscripts $_1$ and $_2$ to refer to radial focussing and defocussing sectors, respectively. We will assume that an equilibrium orbit is made up of alternately inward and outward bending circular arcs, as in Figure 1. The notation indicated in Fig. 1 has become standard. We will take the turning angle β_2 and the radius of curvature ρ_2 in the defocussing sector as negative when the

orbit bends away from the center of curvature as in the Mark I machine. The radius r from the center of the machine to any point on the orbit can for most purposes be taken equal to r_E since β, θ are small.

The following geometrical relationships are evident from the figure, where N is the total number of sectors, and the approximate expressions are valid when the angles are small:

$$N = \frac{2\pi}{\beta_1 + \beta_2} = \frac{2\pi}{\theta_1 + \theta_2} \tag{1}$$

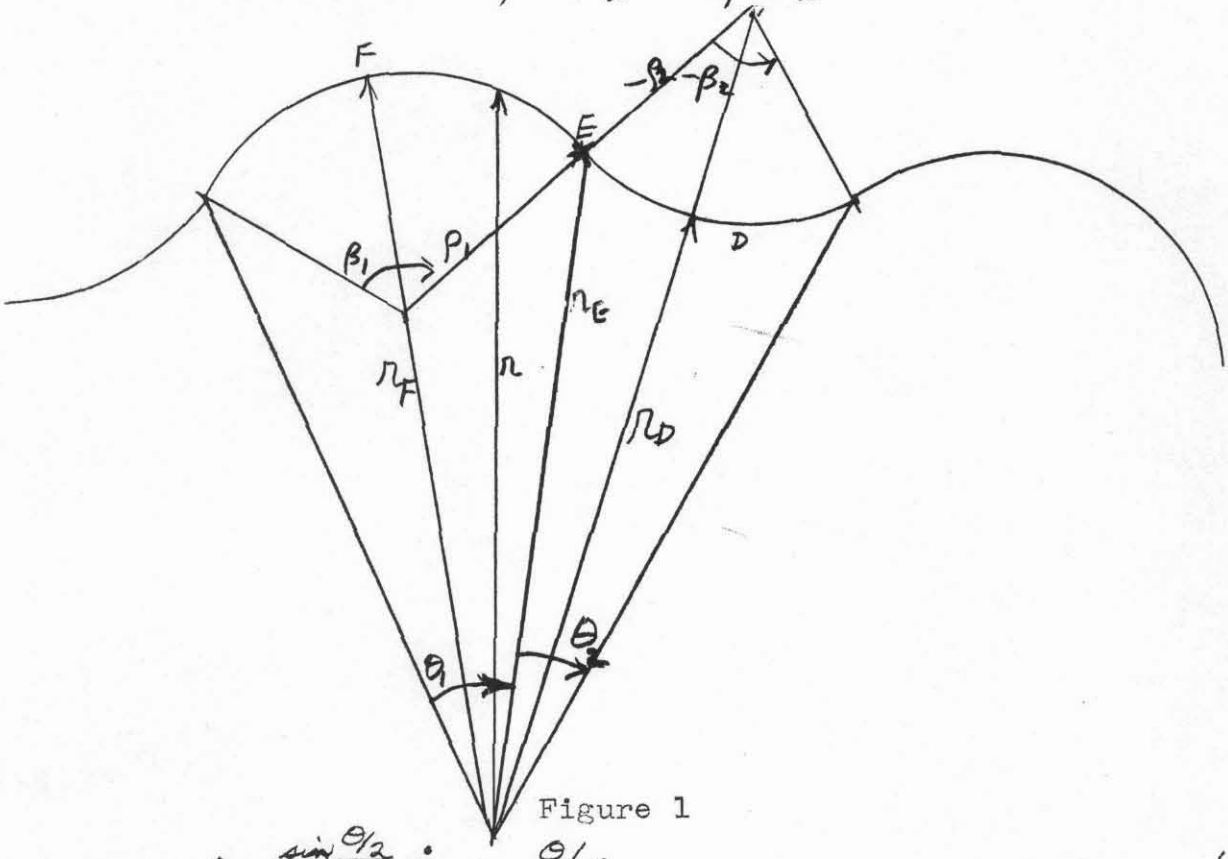

Figure 1

$$\rho = r_E \frac{\sin\theta/2}{\sin\beta/2} \doteq r\,\theta/\beta \qquad \text{(either sector)} \tag{2}$$

The length of either sector is

$$S = \rho\beta \doteq r\theta \tag{3}$$

The total length of orbit is

$$L = N(S_1 + S_2) = 2\pi \frac{\beta_1\rho_1 + \beta_2\rho_2}{\beta_1 + \beta_2} \tag{4}$$

The circumference factor, if $\rho_1 > |\rho_2|$, is

$$C = \frac{L}{2\pi\rho_1} = \frac{\gamma(\Gamma+1)}{\Gamma(\gamma-1)} , \tag{5}$$

where

$$\gamma = -\beta_1/\beta_2 , \tag{6}$$

$$\Gamma = \frac{\theta_1}{\theta_2} \doteq s_1/s_2 . \tag{7}$$

In the Mark Ib machine,

$$\rho_2 = -\rho_1 , \quad \gamma = \Gamma , \quad C = \frac{\gamma+1}{\gamma-1} . \tag{8}$$

The deviation of the scalloped orbit from a circle of radius r_E may be determined by calculating the distances

$$r_F = r_E\left[1 + 2\sin\frac{\theta_1}{4}\left(\cos\frac{\theta_1}{4}\tan\frac{\beta_1}{4} - \sin\frac{\theta_1}{4}\right)\right]$$

$$\doteq r_E\left[1 + \tfrac{1}{8}\theta_1(\beta_1 - \theta_1)\right] , \tag{9}$$

$$r_D = r_E\left[1 - 2\sin\frac{\theta_2}{4}\left(\sin\frac{\theta_2}{4} - \cos\frac{\theta_2}{4}\tan\frac{\beta_2}{4}\right)\right]$$

$$\doteq r_E\left[1 - \tfrac{1}{8}\theta_2(\theta_2 - \beta_2)\right] \tag{10}$$

If $N \gtrsim 50$, $\theta \lesssim 0.063$, $\beta \lesssim 0.31$, the differences between r_F, r_D, and r_E are less than about 0.25%.

We can solve eqs (1), (6), and (7) for θ and β:

$$\beta_1 = \frac{\gamma}{\gamma-1}\,\frac{2\pi}{N} , \tag{11}$$

$$\beta_2 = -\frac{1}{\gamma-1}\,\frac{2\pi}{N} , \tag{12}$$

$$\theta_1 = \frac{\Gamma}{\Gamma+1}\,\frac{2\pi}{N} , \tag{13}$$

$$\theta_2 = \frac{1}{\Gamma+1}\,\frac{2\pi}{N} . \tag{14}$$

We then have:

$$\frac{\beta_1}{\theta_1} = \frac{\gamma(\Gamma+1)}{\Gamma(\gamma-1)} = C, \quad \frac{\beta_2}{\theta_2} = -\frac{\Gamma+1}{\gamma-1} = -\frac{\Gamma}{\gamma}C \tag{15}$$

For Mark I machines, all orbits are geometrically similar, and the ratios

$$\frac{\rho_1}{\nu_E} = \frac{\sin\theta_1/2}{\sin\beta_1/2} \doteq \frac{1}{C} \tag{16}$$

$$\frac{\rho_2}{\nu_E} = \frac{\sin\theta_2/2}{\sin\beta_2/2} \doteq -\frac{\gamma}{\Gamma C}, \tag{17}$$

are independent of energy.

3. Linear orbit theory.

The linearized equations for betatron oscillations about an equilibrium orbit are given by Courant and Snyder (EDC/HSS-1, p.4):

$$\frac{d^2 z}{ds^2} = -\frac{n}{\rho^2} z = \frac{1}{H\rho}\frac{\partial H}{\partial x} z , \tag{1}$$

$$\frac{d^2 x}{ds^2} = \frac{(n-1)}{\rho^2} x = -\left(\frac{1}{H\rho}\frac{\partial H}{\partial x} - \frac{1}{\rho^2}\right) x , \tag{2}$$

where x and z are the deviations from the equilibrium orbit in radial and vertical directions, respectively, and

$$n(s) = -\frac{\rho(s)}{H(s)}\frac{\partial H}{\partial x} , \tag{3}$$

where $H = H_z$ is the magnetic field in the plane of the orbit. In the cases of interest $|n| >> 1$, and the second terms in parentheses in Eq. (2) can be neglected. The distance x is to be measured perpendicular to the orbit at each point, but can, to a good approximation, be measured radially outward from the center of the machine.

If the field is constant along each equilibrium orbit within a half-sector, then by Eqs. (2-9), (2-10)*, the gradients are also very nearly constant along each equilibrium orbit within a half-sector. The index n is then constant within each half sector, and we will designate its values by n_1 and n_2 in the two half-sectors. Since ρ_1, H_1, and $\frac{\partial H}{\partial x}$ are all positive, while ρ_2, H_2, and $\frac{\partial H_2}{\partial x}$ are all negative, n_1 is negative, and n_2 is positive.

The phase transformation matrix for a focussing half-sector, according to Courant and Snyder, is

*The first number in parentheses is the number of the section in which the equation occurs. When the section number is omitted, the reference is to the present section.

$$M_f = \begin{pmatrix} \cos\psi & \frac{s}{\psi}\sin\psi \\ -\frac{\psi}{s}\sin\psi & \cos\psi \end{pmatrix} \tag{4}$$

with

$$\psi = \psi_{1f} = \sqrt{\frac{1-n_1}{\rho_1^2}}\, s_1 , \qquad \text{for radial focussing sector,}$$
$$\psi = \psi_{2f} = \sqrt{\frac{n_2}{\rho_2^2}}\, s_2 , \qquad \text{for vertical focussing sector,} \tag{5}$$

and for a defocussing half-sector

$$M_d = \begin{pmatrix} \cosh\psi & \frac{s}{\psi}\sinh\psi \\ \frac{\psi}{s}\sinh\psi & \cosh\psi \end{pmatrix}, \tag{6}$$

with

$$\psi = \psi_{1d} = \sqrt{\frac{n_2-1}{\rho_2^2}}\, s_2 , \tag{7}$$
$$\psi = \psi_{2d} = \sqrt{\frac{-n_1}{\rho_1^2}}\, s_1 .$$

If we neglect 1 in conparison with n,

$$\psi_{1f} = \psi_{2d} = \psi_1 = \sqrt{\frac{-n_1}{\rho_1^2}}\, s_1 ,$$
$$\psi_{2f} = \psi_{1d} = \psi_2 = \sqrt{\frac{n_2}{\rho_2^2}}\, s_2 . \tag{8}$$

For a full sector, from the beginning of one radial focussing sector to the next, the matrix for radial motion is, then

$$M_x = M_f M_d = \begin{pmatrix} \cosh\psi_1\cosh\psi_2 + \frac{\psi_2 s_1}{\psi_1 s_2}\sin\psi_1\sin\psi_2 & \frac{s_2}{\psi_2}\cos\psi_1\sinh\psi_2 + \frac{s_1}{\psi_1}\sin\psi_1\cosh\psi_2 \\ \frac{\psi_2}{s_2}\cos\psi_1\sinh\psi_2 - \frac{\psi_1}{s_1}\sin\psi_1\cosh\psi_2 & \cos\psi_1\cosh\psi_2 - \frac{\psi_1 s_2}{\psi_2 s_1}\sin\psi_1\sinh\psi_2 \end{pmatrix}. \tag{9}$$

The matrix for vertical motion is obtained from Eq. (9) by interchanging subscripts $_1$ and $_2$. The betatron phase shifts through a sector are

$$\cos\sigma_x = \tfrac{1}{2}\,\mathrm{Tr}(M_x) = \cos\psi_1\cosh\psi_2 + \frac{\xi-1}{2\sqrt{\xi}}\sin\psi_1\sinh\psi_2, \tag{10}$$

$$\cos\sigma_z = \cos\psi_2\cosh\psi_1 - \frac{\xi-1}{2\sqrt{\xi}}\sin\psi_2\sinh\psi_1, \tag{11}$$

where

$$\xi = \left(\frac{\psi_2 S_1}{\psi_1 S_2}\right)^2 = -\frac{\partial H_2/\partial x}{\partial H_1/\partial x} \tag{12}$$

Equations (10), (11), (12) determine the quantities ψ_1, ψ_2, ξ for any orbit in terms of σ_x, σ_z and $S_1/S_2 \equiv \Gamma$. We shall require that all orbits lie at the same point on the necktie, i.e. that σ_x, σ_z shall be the same for all orbits. Given σ_x, σ_z, then ψ_1, ψ_2, ξ are determined as functions of Γ.

In the Mark I machine, Γ is the same for all orbits, so that ψ_1, ψ_2, ξ are the same for all orbits. Since ρ is proportional to S, this implies by Eq. (8) that n_1, n_2 must be the same for all orbits. In the Mark Ib machine, $\xi = 1$, and we have the simple relations

$$\cos\sigma_x = \cos\psi_1\cosh\psi_2 \tag{13}$$

$$\cos\sigma_z = \cos\psi_2\cosh\psi_1 \tag{14}$$

$$\frac{\psi_1^2}{\psi_2^2} = \Gamma = \gamma$$

For a minimum circumference factor, γ should be a maximum. The maximum value of γ on the necktie occurs at the lower left hand corner, $\sigma_x = \pi$, $\sigma_z = 0$. If we take as the closest safe approach to the corner,

$$\sigma_x = \frac{5\pi}{6}, \quad \sigma_z = \frac{\pi}{6}, \tag{15}$$

then we obtain, from Eqs. (13) and (14):

$$\psi_1 = 2.01, \qquad \psi_2 = 1.34, \tag{16}$$

$$\gamma = 1.50, \qquad C = 5.0. \tag{17}$$

In the Mark Ia machine, the maximum value of γ is still about 1.5, and $\Gamma = 1$, so that, by Eq. (2-5), $C = 6$.

4. Magnetic field patterns.

In the Mark I machine, ρ is proportional to r_E. For the radial focussing half-sector, the relation is very nearly

$$\rho_1 \doteq \frac{r_E}{C} . \tag{1}$$

Hence, by Eq. (2-16), if we omit the subscript "E"

$$\frac{dH_1}{dr} \doteq \frac{\partial H_1}{\partial x} = \frac{-n_1 C H_1}{r} \tag{2}$$

and

$$H_1 = H_{o1} (r/r_o)^{-n_1 C} \tag{3}$$

where the subscript "o" refers to the maximum energy orbit. Similarly,

$$H_2 = H_{o2} (r/r_o)^{\frac{n_2 \Gamma C}{\gamma}} \tag{4}$$

If Eq. (3-12) is to hold at all radii, the exponents must be equal, and

$$\frac{n_1}{n_2} = -\frac{\Gamma}{\gamma} \tag{5}$$

$$\frac{H_{o1}}{H_{o2}} = -\delta \tag{6}$$

For Mark Ib, we may set

$$n_1 = -n, \quad n_2 = n, \tag{7}$$

$$n = \frac{\rho^2 \psi^2}{s_2} = \frac{\psi^2}{\beta^2}$$

$$= \frac{(\gamma+1)^2 \psi_2^2}{4\pi^2} N^2 \tag{8}$$

$$H_1 = -H_2 = H_o (r/r_o)^{nC} \tag{9}$$

where we have used Eqs. (203), (2-12), and (3-8). For the case $\sigma_x = 5\pi/6$, $\sigma_z = \pi/6$ this is

$$n = .0113N^2. \tag{10}$$

To a good approximation, the magnetic field in the median plane may be taken as given by Eqs. (3) and (4), where r is the radius from the center of the machine to a point on the orbit. More precisely, we should require that within a half-sector the field be constant along any one orbit and be given at the ends of the half-sector by Eq. (3) or (4). The orbits within the half-sectors will then be exactly circular arcs as shown in Fig. 1, but the gradients will then be about 1/4% too small or too great in magnitude at the centers of the focussing or defocussing half-sectors, and will be too great at the ends of the sectors by a factor

$$\frac{1}{\cos\frac{\beta-\theta}{2}} \doteq 1 + \frac{(\beta-\theta)^2}{8}, \tag{11}$$

or about 1%. The errors at the centers of the sectors are due to the fact that $r \neq r_E$, and those at the ends are due to the fact that $\partial/\partial x$ was replaced by $\partial/\partial r$ in Eq. (2).

Once the magnetic field is specified on the median plane, it is determined throughout the space between the magnet poles by Maxwell's equations. A good approximation to the field pattern can be obtained by neglecting the curvature of the orbits, and requiring that H be the gradient of a harmonic potential function in a vertical plane through the center of the machine.

A suitable potential function is

$$V(r,\varphi) = \frac{H_0 r_0}{nC+1}\left(\frac{r}{r_0}\right)^{nC+1} \sin(nC+1)\varphi, \tag{12}$$

where r, d are polar coordinates in the vertical plane (Fig.2).

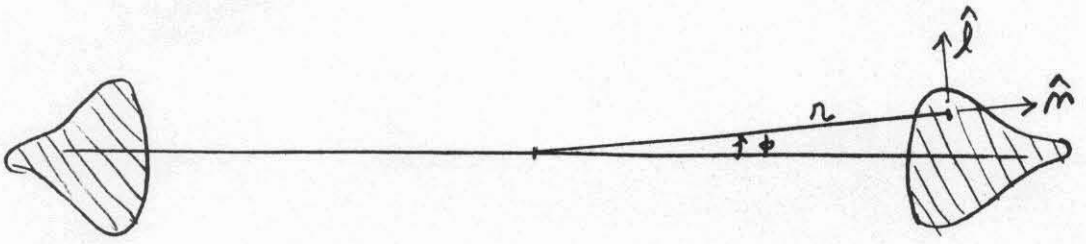

Figure 2

The resulting magnetic field is

$$\vec{H} = \hat{l} H_0 \left(r/r_0\right)^{nC} \cos(nC+1)\varphi + \hat{m} H_0 \left(r/r_0\right)^{nC} \sin(nC+1)\varphi \tag{13}$$

This field has the required form in the horizontal plane $\varphi = 0$.

If we introduce rectangular coordinates x, z, with origin at any point r,o in the horizontal plane, then if x, z $\ll$ r, we can write as a good approximation

$$\vec{H} \doteq \hat{k} H_0 \left(r/r_0\right)^{nC} e^{\frac{nCx}{r}} \cos\frac{nCz}{r} + \hat{i} H_0 \left(r/r_0\right)^{nC} e^{\frac{nCx}{r}} \sin\frac{nCz}{r} \tag{14}$$

where we have also neglected 1 in comparison with nC. This field can in fact be derived from the harmonic potential

$$V(x,z) = \frac{H_0 r_0}{nC}\left(r/r_0\right)^{nC+1} e^{\frac{nCx}{r}} \sin\frac{nCz}{r}. \tag{15}$$

5. Momentum compaction and phase stability

On the equilibrium orbit,

$$pc = eH\rho . \tag{1}$$

Multiplying Eq. (4-3) by $e\rho$, and using (4-1), we obtain

$$pc = p_o c \, (r/r_o)^{nC+1} \tag{2}$$

or

$$r = r_o \left(\frac{p}{p_o}\right)^{\frac{1}{nC+1}} \tag{3}$$

where $n = -n_1$.

This equation determines the donut thickness for any given output and injection energies.

The frequency of revolution is very nearly

$$V = \frac{p}{2\pi m r} = V_o \left(\frac{E_o + m_o c^2}{E + m_o c^2}\right)\left(\frac{p}{p_o}\right)^{\frac{nC}{nC+1}} \tag{4}$$

$$= V_o \left(\frac{p_o^2 + m_o^2 c^2}{p^2 + m_o^2 c^2}\right)^{1/2} \left(\frac{p}{p_o}\right)^{\frac{nC}{nC+1}}$$

At low energies, the second factor is dominant and the frequency increases with energy nearly in proportion to p; at high energies, the first factor dominates, and the frequency slowly decreases as $p^{-\left(\frac{1}{nC+1}\right)}$. The transition energy occurs at

$$p_t = m_o c \sqrt{nC+1} . \tag{5}$$

If N ~ 100, then n ~ 100, by Eq. (4-10), and nC ~ 500, so that

$$E_t \sim p_t c \sim 22 \, m_o c^2 . \tag{6}$$

For protons the transition energy is about 20 Bev, and can be made higher by choosing a larger N. It is very likely that even if the transition energy is somewhat below the output energy, no phase reversal of the rf is required, since the large phase oscillations which occur at the transition energy (and are not objectionable in the D.C. synchrotron) may carry the particles out to the maximum energy orbit.

From Eq. (3), we can calculate

$$\alpha = \frac{r}{n} \frac{dn}{dp} = \frac{1}{\eta C + 1} \quad . \tag{7}$$

Since all equilibrium orbits are similar, the circumference of the orbit is proportional to the radius, the ratio being slightly greater than 2π, and hence Eq.(7), and the last member of Eq. (4) are exact.

6. Design parameters for typical machines.

Parameters have been calculated for a FFAG proton synchrotron with an output energy of 10 Bev. We choose $\sigma_r = 5\pi/6, \sigma_z = \pi/6$ and we assume a maximum magnetic field of 20,000 gauss. Taking 96 sectors we obtain a donut radius of 90 meters, with a radial aperture of 1 meter. The parameters are given in Table 1. Table 2 shows the orbit radius, magnetic field, frequency of revolution, vertical aperture, and some magnetic field equipotentials as a function of energy. The vertical aperture was calculated rather arbitrarily by following the adiabatic damping curve down to a final aperture of 1 cm.

The large change in frequency of revolution could be accomodated by modulating the rf accelerating voltage from 174.7 kc/s to 524 kc/s. Particles would be injected when the oscillator is at 174.7 kc, and would be revolving at slightly below the 9th subharmonic. Particles injected at .5 Mev during the proper phase would execute synchrotron oscillations about an orbit of about .63 Mev. The frequency is then increased to 524 kc/s, when the particle energy will be about 6 Mev. The rf voltage is turned off, and turned on smoothly at 174.7 kc/s, so that the 6 Mev particles would be revolving at about the 3rd subharmonic. At the same time another pulse of particles can be injected. The next fm cycle carries the particles to an energy of about 60 Mev, with a revolution frequency of 174.7 kc/s, from which they are accelerated on the fundamental during the next fm cycle. At each fm cycle, (after the third), a pulse of particles appears at the output energy. If we assume an energy gain of 500 Kv per turn in the final cycle, a pulse repetition rate of about 10 cycles per second. Since no r.f. tracking is required, it may be possible to use a mechanically modulated high

Q cavity and obtain 500 Kv across a single r.f. gap. In this case it may be possible to dispurse with the injector altogether and locate the ion source just ahead of the accelerating gap.

A treatment of straight sectors is the subject of a forthcoming report.

Table 1.

Typical Design Parameters Mark Ib

Output energy 10 Bev

Injection energy 0.5 Mev

Max doughnut radius 90.75 m

radial aperture 1 m

vertical aperture at injection 19 cm

vertical aperture at 20 Bev 1 cm

σ_r	$5\pi/6$
σ_z	$\pi/6$
γ	1.5
N	96
n	104
C	5

Table 2

Energy Mev	Orbit radius m	H gauss	Vertical Aperture cm	ν kc/s	Magnet Equipotential Separation cm	
10,000	90.75	20,000	1.00	524	1.00	
3,000	90.65	7,000	1.69	511	2.87	
1,000	90.50	3,100	2.54	462	6.47	
300	90.35	1,500	3.67	345	13.56	
100	90.25	820	4.95	226	24.6	5.00
30	90.15	440	6.75	134	∞	9.44
10	90.07	250	8.91	77.4		20.8
3	89.97	140	12.04	42.5		∞
1	89.85	80	15.9	24.5		
.5	89.80	57	18.9	17.4		